Particulate number and NO_x trade-off comparisons between HVO and mineral diesel in HD applications

Thomas Bohl[a], Andrew Smallbone[a], Guohong Tian[a], A.P. Roskilly[a]

[a] *Sir Joseph Swan Centre for Energy Research, Newcastle University, Newcastle upon Tyne, NE1 7RU, UK*

Abstract

The increase in worldwide greenhouse gas emissions and costs for fossil fuels are forcing fuel suppliers and engine manufacturers to consider more sustainable alternatives for powering internal combustion engines. One very promising equivalent to mineral diesel fuel is hydrotreated vegetable oil (HVO) as it is highly paraffinic and offers similar combustion characteristics. This fuel offer the potential of not requiring further engine hardware modification together with correspondingly lower exhaust gas emissions and better fuel consumption than mineral diesel.

In this paper the spray and combustion characteristics of HVO and its blends are investigated and compared with mineral diesel (European standard). Evidence of the reported reductions in NO_x emissions has proven contradictory with some researchers reporting large reductions, whilst others measured no differences.

This paper reports the results from comparison of three different experimental tests methods using diesel/HVO binary fuel blends. The macroscopic spray characteristics have been investigated and quantified using a constant volume spray vessel. Engine performance and exhaust emissions have also been characterised using a HD diesel engine in its original configuration (mineral diesel fuel-ready) and then in a recalibrated configuration optimised for HVO fuel.

The results show that the engine injection control and also the fuel quality can influence the formation of NO_x and particulate matter significantly. In-particular a potential pilot injection proved highly influential upon whether NO_x emissions were reduced or not. When optimising the fuel injection, a reduction in NO_x emissions of up to 18 % or reductions of PN of up to 42 – 66 % were achieved with simultaneous savings in fuel consumption of 4.3 %.

Keywords: HVO; Spray characteristics; Constant volume vessel; Engine performance; NO_x; Particulate Number

1 Introduction

Hydrotreated vegetable oil (HVO) is a highly paraffinic diesel-like biofuel, with the chemical structure C_n H_{2n+2}, processed from vegetable oil by adding hydrogen in a catalytic reaction. Hydrotreated fuels are also called "renewable diesel fuels" and the term biodiesel is usually avoided since this is more conventionally used for fatty acid methyl esters (FAME) produced by transesterfication [1]. HVOs are mixtures of paraffinic hydrocarbons without sulphur or aromatic contents. They are characterised by a higher cetane number (CN) and lower density than conventional mineral diesel. It has been reported that no engine modification or additional service of the engine is necessary and up to 30% of HVO can be added into European diesel fuel (EN590), and even more into American diesel fuel (ASTM D975) to still meet legislative fuel standards. Even pure HVO fuel is already being utlised for public transport, such as city buses [1].

An illustration of the production process is shown in Figure 1.

In the first step, the triglyceride is hydrogenated and broken down into mono-glycerides, di-glycerides and carboxylic acids. These intermediates are then formed into *n*- and *iso*-alkanes by either hydrogenation (with no carbon removal) or decarboxylation and decarbonylation (both removing a carbon from the initial intermediate) [2]. The by-products are water, carbon monoxide, carbon dioxide as well as naphtha, which is a group of liquid hydrocarbons which could be used for heating and energy requirements. The CO and CO_2 can react further to produce methane, another useful by-product. In the presence of a zeolite catalyst [3], reaction temperatures and pressures are between 300 and 360 °C and 50 to 180 bar pressure, respectively. The composition of the products to their desired state is dependent on the above reaction temperatures.

The first commercial scale HVO plant with a 170,000 ton/year capacity was built in the summer 2007 at Neste Oil's Porvoo oil refinery in Finland [1]. Two years later, Neste started a second plant with the same capacity. In 2010 and 2011 two large scale plants in Rotterdam and Singapore with an annual capacity of 800,000 ton were commissioned. Currently HVO plants are mainly integrated into oil refinery plants, but companies have started developing larger stand-alone units around the world for large-scale production [4]. The costs of producing HVO are in some studies is stipulated to be about 50% the transesterfication processing costs [5]. Kalnes, *et al.*, however, stated that the overall economics will depend on feedstock costs and by-product revenues [6]. Sunde, *et al.* reported in their studies that HVO made from waste or by-products outperforms FAMEs (fatty acid methyl ester) and BtL (biomass-to-liquid) in respect to costs and environmental life cycle impacts [5]. However, feedstock availability and logistics are currently limiting factors and other raw materials must be used. HVO has lower viscosities, lower cloud points and therefore better storage and cold flow properties

than FAMEs. Also the relatively high heating value and CN makes HVO a very high-quality fuel for potential utilisation in the transportation sector. Nevertheless, a potential drawback for HVO is that lubricity is poorer and additives have to be used to increase lubrication properties [7].

Some researchers have tested HVO on different engines to gain an understanding of its combustion and exhaust formation behaviour. Kuronen, *et al.* tested neat HVO on two heavy duty engines and two city buses and compared the results with EN 590 diesel fuel [8]. For HVO, the particulate mass (PM) was reduced between 28 and 46%, NO_x was reduced by 7 to 14% and THC and CO emissions decreased by 0 - 48% and 5 to 78%, respectively. In a later study, they used a 6 cylinder 8.4 litre DI engine at several speeds and loads and carried out an injection timing sweep [1]. They found that by retarding the injection, the smoke- NO_x trade-off shifts towards higher smoke numbers and lower NO_x values. Also, retarding the injection resulted in higher bsfc (brake specific fuel consumption), but much lower NO_x emissions. They concluded that a clear reduction in NO_x and smoke emissions as well as fuel consumption (mass-based), but higher volumetric fuel consumption was due to the lower fuel density. Pflaum, *et al.* investigated emission formation of neat HVO and mineral diesel in a CI 2 litre four cylinder test engine and on a chassis dynamometer test [9]. Their results revealed that HVO has the potential to reduce PM, THC and CO emissions up to 50% as it is free of aromatic compounds. The NO_x emissions, however, only showed a slight reduction compared to fossil diesel. Ratanen, *et al.* tested several HVO blends (5, 15, 20 and 85 vol%) and compared them with conventional diesel [10]. They pointed out that both regulated and non-regulated emissions decreased with increasing HVO ratios. However, a clear reduction of NO_x was not observed. Similar results have been found by Kim, *et al.* testing HVO and iso-HVO in a light duty diesel engine and no significant differences in NO_x are observed when HVO blend ratio was increased [11]. A study has been carried out by Toyota investigating the effect of single and multi-injection with HVO and EN590 diesel and they found out that with a single injection NO_x emissions are reduced up to about 10 % with HVO, while with a pilot injection no significant reductions are found [12]. The conclusion was that with a pilot injection, the start of the main fuel ignition is very similar with HVO and mineral diesel and the heat release curves were identical.

Very few papers related to spray characteristics have been published. Hulkkonen, *et al.* compared the macroscopic spray characteristics of HVO and mineral diesel [13]. An injector with two different nozzle diameters of 0.08 and 0.12 mm in a common rail fuel system with rail pressures of 450, 1000 and 1980 bar were used. They concluded that neither the type of fuel, nor the orifice diameter had an effect on the spray penetration. They further found out that the cone angle of HVO is greater than that of diesel, probably due to lower viscosity of HVO. The spray angle also increased with a larger orifice diameter, but diminished with higher injection pressures. Finally they concluded that the macroscopic spray characteristics of HVO are similar to GtL (gas-to-liquid). The effect of pure HVO on

macroscopic spray parameters in a DI engine were studied by Sugiyama, *et al.* [12]. Their results revealed that the Sauter mean diameter, spray penetration and spray angle were similar for conventional diesel and HVO. Chen, *et al.* investigated the microscopic and macroscopic spray behaviour of HVO and other biofuels and concluded that HVO has a much smaller SMD than diesel and that the effect of injection pressure on spray angle was not obvious for all tested fuels [14]. Overall, the amount of research conducted on HVO is small despite HVO being a very promising future fuel. In reviewing the literature, it was concluded that the results of HVO, such as exhaust emission and spray characteristics are heavily dependent on the B0 benchmark fuel and the injection conditions used in the study. Whilst almost all studies the properties of the benchmark fuel were all within the EN590 limits, the differences in viscosity, CN and aromatics content all varied significantly and thus affected the results accordingly. In this work, the macroscopic spray characteristics, engine test bench performance and injection recalibration has been carried out with neat HVO and its blends benchmarked with the same reference fuel. The novelty of this study is the holistic investigation of spray and combustion analysis for a heavy-duty application using HVO and its blends.

2 Experimental setup and procedure

2.1 Constant volume vessel

A medium pressure, high temperature combustion vessel was used to investigate the spray and combustion characteristics using a high-speed direct photography technique. The vessel is made of Inconel alloy and is resistant against corrosion and oxidation and suited for extreme environments and can be subjected to pressure of 100 bar and temperatures of up to 500 K. The constant volume vessel (CVV) has four optical accessible windows with 100 mm viewing size and further consists of an external 4.5 kW ceramic band heater.

The fuel injection system contains an air-driven high pressure fuel pump, where the fuel can be pressurised and stored in a common rail up to 1800 bar. A standard Bosch solenoid injector with a 0.16 mm single-hole nozzle was mounted onto the vessel and can be triggered using an external solenoid driving box. A PHANTOM V710 monochrome charge-coupled device (CCD) camera captured the spray images with a resolution of 256x256 pixels, a capturing speed of 70,000 frames per second (fps) and an exposure time of 5 ns. The camera was synchronised with the injector by using the same triggering signal. A Nikon AF-S Nikkor lens with a focal length of 70-200 mm and a maximum aperture of f/2.8 was attached to the camera. A 500 W xenon light source on the opposite window ensures constant background light for the camera. The background pressure and temperature of the vessel is monitored and controlled by a control panel supplied by the vessel manufacturer. The

CVV set up including high pressure fuel system and optical diagnostic devices are illustrated in Figure 2.

After the experimental data were recorded, a MATLAB program was used to post-process the results. This program was developed to automatically measure cone angle, penetration length and spray area of consecutive images of the spray. Figure 3 illustrated the two main spray characteristics, cone angle and penetration length, measured by the program. The "Spray Tip Penetration Length" is defined as the axial distance from the nozzle exit to the tip of the spray.

The "Cone Angle" was defined here as the angle formed by two tangential lines touching the outer boundaries of the spray on either side and joining together at the nozzle exit. The cone angle was determined by measuring the angle between nozzle exit and the first and last pixel of each row and obtaining the observed average. The spray area is defined as the area covered by the fuel plume at chamber conditions. To calculate the spray area the binary image (with the same threshold limit as for the penetration and cone angle) was used to sum up all black pixel within the spray plume. The principle is illustrated in Figure 4 for the three measurements, penetration distance, cone angle and surface area.

A single-hole nozzle with an orifice diameter of 0.16 mm was selected for the study. The vessel was filled with compressed nitrogen (N_2), heated up to 100 °C and pressurised to 70 bar resulting in a chamber density of approximately 65.5 kg/m^3. The common rail pressure was set to 1800 bar and an injection duration of 0.6 ms was selected. The chamber density, rail pressure and injection duration have been chosen specifically as they are representing the injection conditions at the end of the compression stroke in the HD diesel engine used in this study. The ten injection events were studies per test point each with around 70 images obtained within 1 ms after the start of injection. For all 700 images, the spray penetration, spray cone angle and spray surface area were determined using the custom algorithm written in MATLAB and described above.

The fuel quantity per injection stroke has been measured for each fuel by injecting 1000 times into a small container and weighing it.

2.2 Engine test bed

The engine, which was built and used in this research, is a four-cylinder Cummins ISBe5 heavy duty, direct injection, four-stroke diesel engine with a high pressure common rail fuel system. The common rail system has a maximum pressure of 1800 bar and is connected to solenoid fuel injectors. The engine is equipped with a waste gate turbocharger and an air to water intercooler. The engine has a

rated power output of 155 kW with a maximum torque level of 760 Nm between 1400 and 1800 rpm and is connected to an eddy-current W230 dynamometer to control torque and speed of the engine. The displacement volume is 4.5 L with a bore diameter of 107 mm and a stroke length of 124 mm.

The exhaust gas is connected to a Horiba MEXA-1600D gas analyser to measure NO_x, CO, CO_2, O_2 and HC emissions. In the analyser, the NO_x is measured using a chemiluminescence detector (CLD), HC with a flame ionisation detector (FID), CO/CO_2 with a non-dispersive infra-red analyser (NDIR) and O_2 with the magnetic-pneumatic method (MPD) [16]. A Horiba MEXA-1000 SPCS particle counter will be used to count the particle numbers in real time using Laser Based Condensation Particle Counting (CPC) [17].

For combustion analysis, an AVL water-cooled, high-speed pressure transducer QC34C is mounted in cylinder #3 to record the in-cylinder pressure. An optical crank angle encoder 365C supplied by AVL is mounted at the free end of the crank shaft to provide crank-angle based timing information for the pressure transducer. From the pressure and crank angle data, the indicated mean effective pressure (imep), heat release profile and combustion duration can be derived. The pressure sensor signal is converted from an electrical charge into a proportional voltage signal and amplified through an AVL 1-channel charge amplifier and recorded through a high-speed NI data acquisition card PCI-6251. An external fuel conditioning system has been installed to cool down the fuel return flow and measure the bsfc using an integrated Coriolis flow meter. A schematic diagram of the engine setup is shown in Figure 5.

For the engine tests, the European Stationary Cycle (ESC) was used and it is illustrated in Figure 6. At each test point, the emissions have been recorded over a period of 120 seconds and the crank-angle based in-cylinder pressure was logged over a period of 300 cycles.

The test fuels for the work were supplied by BP (UK) in blends of B10, B20, B50 and B100. A comprehensive analysis of the fuel properties was carried out. The main fuel properties are illustrated in Table 1.

3 Results and discussion

3.1 Spray test results

3.1.1 Spray penetration

The averaged spray penetration for B0, HVO B100 and B50 are plotted in Figure 7 (top). The graph can be divided into three stages. The initial part shows a linear phase, which is identical for all three fuels. In the second phase the injection advances as a function of square root over time. In the third phase, the injection event itself has stopped after 0.6 ms and the spray plume continues travelling with at a similar speed across the chamber. The start of injection has been referenced to the origin as there were slight differences in the visual start of injection. The spray penetration at the start is very similar for all fuels until the curve for HVO B50 and B100 gradually starts to deviate from the B0 curve. The overall lower spray penetration curve for HVO has also been observed by other researchers [13, 14]. The lower fuel density of HVO as well as the smaller SMD are the most likely sources for the lower penetration length in a high density chamber as they carry less momentum than heavier and larger droplets.

3.1.2 Spray cone angle

Figure 7 (middle) shows the evolution of the cone angle of the three fuels. The spray angle of all fuels is relatively constant between 21° and 25° during the full injection duration. In particular, the initial phase shows very constant spray angles for all fuels until the spray breakup point is reached. After that, the spray angle is widest for HVO B100 followed by B50. Similar observations were made by other researchers [13, 19]. Kitano, *et al.* explained the wider cone angle and smaller SMD with GtL, which is very similar to HVO, was related to the lower viscosity [19]. Nevertheless in this study the viscosity of HVO and B0 were almost identical, and the smaller SMD and therefore wider cone angle are also affected by the lower fuel density [20].

The wider cone angle, but shorter penetration suggest that HVO is distributed more evenly in the chamber and together with the lower SMD (and therefore faster evaporation rate), the fuel-air mixing is improved. This will imply that after a constant ignition delay, the premix combustion phase will take place more rapidly, potentially resulting in issues with engine noise and NO_x emissions.

3.1.3 Spray surface area

As in the engine, volumetric-based injection is taking place, the lower fuel density and higher heating value of HVO effect the energy injection rate. Figure 7 (bottom) shows the spray area per unit energy. The first part of the graph is similar for HVO and B0 fuel as not much fuel has been injected until the spray breakup takes place. In the second phase, the HVO graph deviates from the mineral diesel curve mainly due to the lower fuel injection rate and wider cone angle providing a greater surface area for the gases to mix. This means the local fuel concentration in the chamber is lower, air-fuel mixing is improved and higher heat release rates at the start of combustion would be expected. However, the

higher CN of the fuel may well offset this observation, resulting in an earlier ignition and therefore the heat release rates from the premix phase might be reduced. This explains why some researchers note large reductions in NO_x emissions, while others report no differences as the NO_x formation is not just determined by the ignition delay, but also by the injection control strategy of the engine. This observation is explored in more detail in the engine tests (in paragraph 3.2.3).

3.2 Unmodified engine test comparison

The objective here was to quantify how the engine performance and exhaust gas emissions might respond to the different fuel blends in the event that the mineral diesel fuel was simply replaced by an end-user for HVO and HVO/mineral diesel blends.

3.2.1 Engine performance

The average power output at full load and the fuel consumption across the whole test cycle is shown in Figure 8. The error bars represent the standard deviation around the mean value. In general, the reduction in power and fuel consumption follows a linear trend. With increasing HVO blends, the engine power is reduced marginally from 135.6 kW to 135 kW due to the lower fuel density and therefore lower volumetric heating value. However, the differences are very small and in practice would not be noticeable by an end-user, it can therefore be concluded that full power can be achieved even with HVO B100. Fuel consumption reduces with increasing blend ratio from 217.5 g/kWh to 212.5 g/kWh resulting in fuel savings of 2.3 %. The reduction in fuel consumption corresponds to the higher mass-based heating value (2.4 %) of HVO.

3.2.2 Engine exhaust emissions

Figure 9 shows the specific NO_x and particulate number (PN) emissions over the whole ESC cycle with increased HVO fractions. The NO_x emissions were not affected by increased blend ratios, however the PN emissions did decrease with increasing concentrations of HVO. In terms of NO_x emissions, the largest reduction was achieved with B50 fuel emitting 2.1 % less NO_x than the benchmark. The highest increase in NO_x was observed with B20 fuel of 1.5 % above benchmark. PN reductions were highest at B20 with 17 % followed by B100 with 14% compared to B0 benchmark.

With B20 fuel, the NO_x emissions were observed to be greater than the trend whereas the PN emissions were reduced simultaneously. This observation was investigated further and a combustion analysis showed that at B20, the SOC was about 0.5 CAD later compared to the SOC at B10, B50 and B100. With more time for the fuel-air mixture to premix, higher NO_x and lower PN might be

expected. Also the end of combustion (CA90) is relatively early and the diffusion combustion phase is reduced for this particular point. The combustion duration versus blend ratio has been plotted in Figure 10 and a correlation between combustion duration and particulate emissions can be drawn.

The specific CO and THC emissions are shown in Figure 11. Both reduced with increasing HVO blend with the maximum reduction of 29 % for CO and 61 % in THC. The reduction in CO was attributed to the better fuel-air mixing observed during the spray tests thus minimising any overly fuel-rich zones. In addition, the absence of aromatics would also be expected to affect CO formation as they require higher temperatures to break down and oxidise. The THC are reduced due to lower distillation curve of HVO providing a more complete evaporation at injection and therefore better combustion, furthermore the lack of aromatics content would also be expected to reduce hydrocarbon emissions in the exhaust gas.

3.2.3 Combustion analysis

To analyse the combustion of HVO in comparison with mineral diesel, the heat release rate (HRR) of various test points within the ESC cycle (Figure 6) has been selected as representative to provide more insight into the combustion heat release rates.

Figure 12 shows the HRR of B0 and HVO at test point #2 at engine speed A (1490 rpm) and full load (730 Nm). The shape of the HRR curve is very similar for B0 and HVO and the difference in the higher CN of HVO has no observable effect on ignition delay, neither for the pilot nor main injection events. Schaberg, *et al.* reported that the differences in ignition delay (ID) between a high-CN fuel and a low CN fuel diminishes with higher in-cylinder pressure and temperature [22]. Figure 13 shows the difference in ID as a function of the internal gas temperature and pressure, which indicates that a difference in CN is more effective at lower engine loads. Whilst the presented diagram was generated for GtL fuel, it is also valid for HVO as many of its fuel properties are identical and differences in their chemical structure are considered small [1, 8-10, 21, 23].

At point #2, NO_x emissions proved constant and PN is reduced by 7 % and 14 % for HVO B50 and B100, respectively. This shows that the reductions in PN were not due to an earlier SOC or shorter ID, but were due to an absence of aromatics and possibly the lower distillation curve of HVO.

Figure 14 shows the HRR at the same speed but low load of 200 Nm and the effect of CN is seen for pilot injection. However, the ID for the main injection is nearly zero for all fuels showing that the pilot injection has raised the internal gas temperature to a high enough value that the CN does not affect the main combustion phase. This explains why the NO_x emissions are not reduced significantly

on this engine, but can still be reduced in other engines with alternative control strategies. This is in agreement with the work carried out by Toyota showing that NO_x emissions are reduced with HVO when a single injection was used, but NO_x emissions are unchanged once a pilot injection was added [12].

The NO_x emissions are again fairly constant for the three different fuels and PN reduces by 9.9 % and 24.5 % with B50 and B100, respectively.

Figure 15 shows the HRR at 1855 rpm and 730 Nm (point #8). At higher engine speed, the higher CN of HVO leads to shorter ID at both pilot and main injection. The NO_x increased slightly by 6.7 % and 5% for HVO B100 and B50, respectively. This is potentially due to the slightly earlier increase in heat release for the main combustion and higher peak pressures and temperatures for HVO B50 and B100. The PN emissions are reduced by 3.7 % and 8 %, respectively.

Finally, the heat release rate at 1855 rpm and 200 Nm (point #9) is shown in Figure 16. The NO_x emissions remained unchanged, except that the B50 series seems to have lower NO_x emissions in general, which itself is a potentially a result of the late SOC and combustion duration presented in Figure 10 and described above. The PN emissions have been reduced with B100 and B50 by 6 % and 21 %, respectively and therefore similar to 1490 rpm and low load in Figure 14.

The engine employed in this study had an average ID (ignition delay) of 3.72 CAD for HVO B100 and 5.25 CAD for B0. At average speed of 1855 rpm this is equivalent to an ID of 0.33 ms and 0.47 ms, respectively. However, the ID time is only relevant for at the pilot injection phase and no difference in ID was observed for the main injection. Therefore, the increased CN had no observable effect on the NO_x reduction when a pilot injection took place and the internal gas temperature is already very high. Basically, the pilot injection is compensating for the low CN in some point and therefore the benefit of high CN of HVO cannot develop its full potential. Hartikka, *et al.* explained the lower absolute emission reductions with HVO with more recent engines, such as EURO IV, V and VI, due to the aftertreatment system and the more precise and complex control strategy of the engine [21]. As new aftertreatment is equipped to this test engine, the addition of the pilot injection is the main contributor to the lower emissions reductions. Also the quality of the benchmark fuel itself will play a major effect in the reduction potential of HVO. Especially the aromatics content and the CN of mineral diesel can vary significantly and affect the any emissions benchmark.

The lower adiabatic flame temperature in the absence of aromatics is often used as an explanation for lower NO_x emissions of HVO [13, 21, 22, 24]. It is more likely that the injection control strategy of the engine is also very important for differences in NO_x emissions. This is in agreement with the

statement bv Hartikka, *et al.* that higher NO_x reductions have often been found in older engines, which are equipped with a more simple injection strategy [21]. Also passenger vehicles fuelled with HVO show less NO_x improvement with HVO than heavy duty engines, which could easily be associated with employing a pilot injection strategy in the engines used in those passenger cars.

3.3 Engine recalibration options

As it was concluded that emissions are most directly influenced by the injection strategy of the engine itself, specific test points over the ESC cycle were chosen for re-calibration by changing the start of injection (SOI) and rail pressure (RP) with HVO B100 fuel.

The three points #7, #3 and #4 presented in Figure 6 have been chosen for optimisation and a Design of Experiment (DoE) according to Figure 17 has been developed around the original manufacturer's configuration. Each optimisation was carried out three times and offered sufficient repeatability in terms of fuel consumption, exhaust emissions and in-cylinder pressure data.

Figure 18 and Figure 19 illustrate the NO_x and PN emissions of HVO for the three different test points in relation to the SOI and RP. While the NO_x emissions show a linear trend with changes in SOI and RP, the PN emissions follow a quadratic trend for all test points. This is in agreement with the study of Su, *et al.* who investigated the effect of injection pressure on spray SMD and particulate emissions. They found that the correlation between injection pressure and SMD is linear, but the effect of SMD on particulate emissions is non-linear and seems to follow a quadratic trend [25]. The observed NO_x emissions increased with advanced injection as the peak pressure was closer to TDC and therefore cylinder temperature is increased. Also, the NO_x emissions reduced with reducing rail pressure. This can be explained by the lower kinetic energy available and therefore smaller droplet size distribution of the fuel. This decelerates fuel atomisation and evaporation rates, and the heat release from premix combustion phase is reduced. However, the reduction in NO_x due to the RP is small.

At point 7 (low engine load) the PN emissions increased with retarding injection timing. When increasing the engine speed and load (point #3) this is still the case, but at a much lower magnitude. At higher loads, the trend falls to a reduction in PN emissions with retarded injection. This is an interesting observation and the combustion duration follows exactly the same trend resulting in longer combustion at low load when injection is retarded, but longer duration at high load when injection is advanced. The PN emissions were increased significantly when rail pressure is reduced due to the higher SMD at lower injection pressure and therefore higher particulate emissions. As the benefit of reducing rail pressure in terms of NO_x is small, but the penalty on PN emissions is huge, it can already

been concluded that reducing rail pressure is not an effective strategy for recalibrating the engine control system.

A NO_x, PN and fuel consumption model has been established for various rail pressure and SOI at all three test points. In line with the observations/methods of Su, *et al.* [25], for the NO_x emissions and fuel consumption a linear correlation and for the PN emissions a quadratic correlation has been employed. An example of the NO_x and PN model as a contour plot are shown in Figure 20 and Figure 21 for test point #4.

With these models, a NO_x -PN trade-off curve has been generated showing the lowest PN emissions at each NO_x value. At each of these points, the corresponding fuel consumption has been calculated. The trade-off curves for all three points are illustrated in Figure 22 including their original control settings and the benchmark emission of B0 EN590 fuel.

As mentioned previously, using the RP to reduce as the penalty in PN is not advisable as it exceeds the benefits of reducing NO_x. Increasing the RP could be advantageous, but due to hardware restrictions this was not technically possible in this study. Thus, the trade-off curve was considered only at maximum rail pressure and runs from advanced injection to retarded injection were carried out. The highest reductions in NO_x can be achieved by retarding the SOI by 3.0 CAD and the reduction potential is 16.9 %, 18.4 % and 17.9% for point #7, #3 and #4, respectively. The corresponding PN emissions are 623 %, 174 % and 0 %, respectively, higher than the B0 benchmark. The lowest PN emissions can be achieved when advancing the injection timing by 3.0 CAD and reductions of 66% and 42 % are possible for point #7 and #3. The corresponding NO_x emissions are 10.8 % and 2.3 % higher, respectively. At point #4, a distinctive minimum is found at the lowest PN emissions are found when retarding the injection by 2.7 CAD. At this point the PN emissions can be reduced by 36 % and NO_x emissions by 9.9 %. The brake specific fuel consumption follows a linear trend towards advanced injection. The highest savings can therefore be achieved at advanced injection with a lower fuel consumption compared to B0 of 2%, 3.5 % and 4.3 % for point #7, #3 and #4, respectively.

4 Conclusions

Vast differences in exhaust emissions using HVO compared to mineral diesel have been observed in recent papers. One of the main reasons for this was the fuel properties of the benchmark EN590 minerial diesel fuels themselves, which can change significantly, in particular with aromatics content, viscosity and CN. All these parameters will affect the engine-out NO_x and particulate emissions. In

addition, the engine control strategy is different for every engine and it was concluded that the injection control strategy is responsible for the main differences in exhaust gas emissions. The following further conclusions have been made:

- The penetration distance of HVO is shorter than mineral diesel due to lower SMD and fuel density carrying less momentum during the injection.
- The cone angle of HVO is wider than B0 for the same reasons as the penetration.
- The fuel-air mixing of HVO is better than B0 due to larger cone angle and lower local fuel concentration in the chamber. This will affect the premix combustion and NO_x emissions. The shorter ID of HVO might counteract this effect in some engines.
- No significant power loss appears with HVO. The bsfc can be reduced by up to 2.3 % using neat HVO. The corresponding mass-based heating value is 2.4 %.
- No reductions in NO_x emissions have been observed, but a PN emissions have been reduced by 14 % with increasing HVO blends.
- CO and THC emissions are reduced with increasing HVO blend due to better fuel-air mixture, absence of aromatics and lower distillation curve.
- The shape of the HRR is very similar for B0 and HVO for all test points. The ID is only really affecting the pilot combustion, but the high internal gas temperature at the point of main injection diminishes the effect of higher CN.
- Reducing rail pressure when recalibrating the engine is not beneficial as particulate number is increasing rapidly while the reduction in NO_x emissions in relatively low. When recalibrating the ECU the rail pressure should only be increased (if physically possible) and SOI retarded.
- NO_x emissions follow a linear trend when SOI and RP are changed. For PN emissions however a quadratic trend has been found when SOI and RP are changed.
- Max NO_x reductions of around 18 % with severe penalty in PN when retarding injection fully.
- Max PN reductions of 42 % to 66 % when advancing injection fully. At high load a distinctive minimum provides maximum NO_x and PN emissions of 9.9 % and 36 %, respectively, at the same time when retarding injection by 2.7 CAD.
- Fuel consumption can be reduced by up to 4.3 % below EN590 benchmark.

Acknowledgement

The authors kindly thank Cummins Ltd UK for their financial and technical contribution towards this work. Also, this study was supported by EPSRC scholarship and loan of the camera equipment (EP/J500288/1).

References

1. Aatola, H., M. Larmi, T. Sarjovaara, and S. Mikkonen, *Hydrotreated vegetable oil (HVO) as a renewable diesel fuel: trade-off between NOx, particulate emission, and fuel consumption of a heavy duty engine.* SAE Technical paper, 2008. **2008-01-2500**.
2. Huber, G.W., P. O'Connor, and A. Corma, *Processing biomass in conventional oil refineries: Production of high quality diesel by hydrotreating vegetable oils in heavy vacuum oil mixtures.* Applied Catalysis a-General, 2007. **329**: p. 120-129.
3. Simacek, P., D. Kubicka, I. Kubickova, F. Homola, M. Pospisil, and J. Chudoba, *Premium quality renewable diesel fuel by hydroprocessing of sunflower oil.* Fuel, 2011. **90**(7): p. 2473-2479.
4. Neste, O.I.L., *Hydrotreated vegetable oil (HVO)-premium renewable biofuel for diesel engines.* 2014.
5. Sunde, K., A. Brekke, and B. Solberg, *Environmental Impacts and Costs of Hydrotreated Vegetable Oils, Transesterified Lipids and Woody BTL-A Review.* Energies, 2011. **4**(6): p. 845-877.
6. Kalnes, T.N., K.P. Koers, T. Marker, and D.R. Shonnard, *A Technoeconomic and Environmental Life Cycle Comparison of Green Diesel to Biodiesel and Syndiesel.* Environmental Progress & Sustainable Energy, 2009. **28**(1): p. 111-120.
7. Hoekman, S.K., A. Gertler, A. Broch, and C. Robbins, *Investigation of biodistillates as potential blendstocks for transportation fuels.* CRC AVFL-17, Final Report June, 2009.
8. Kuronen, M., S. Mikkonen, P. Aakko, and T. Murtonen, *Hydrotreated vegetable oil as fuel for heavy duty diesel engines.* SAE Technical Paper, 2007. **2007-01-4031**.
9. Pflaum, H., P. Hofmann, B. Geringer, and W. Weissel, *Potential of Hydrogenated Vegetable Oil (HVO) in a Modern Diesel Engine.* SAE Technical Paper, 2010. **2010-32-0081**.
10. Rantanen, L., R. Linnaila, P. Aakko, and T. Harju, *NExBTL-Biodiesel fuel of the second generation.* SAE Technical Paper, 2005. **2005-01-3771**.
11. Kim, D., S. Kim, S. Oh, and S.-Y. No, *Engine performance and emission characteristics of hydrotreated vegetable oil in light duty diesel engines.* Fuel, 2014. **125**: p. 36-43.
12. Sugiyama, K., Goto, I., Kitano, K., Mogi, K. et al, *Effects of Hydrotreated Vegetable Oil (HVO) as Renewable Diesel Fuel on Combustion and Exhaust Emissions in Diesel Engine.* SAE Technical Paper, 2011. **2011-01-1954**.
13. Hulkkonen, T., H. Hillamo, T. Sarjovaara, and M. Larmi, *Experimental Study of Spray Characteristics between Hydrotreated Vegetable Oil (HVO) and Crude Oil Based EN 590 Diesel Fuel.* SAE Technical Paper, 2011. **2011-24-0042**.
14. Chen, P.C., W.C. Wang, W.L. Roberts, and T.G. Fang, *Spray and atomization of diesel fuel and its alternatives from a single-hole injector using a common rail fuel injection system.* Fuel, 2013. **103**: p. 850-861.

15. Taşkiran, Ö.O. and M. Ergeneman, *Experimental Study on Diesel Spray Characteristics and Autoignition Process.* Journal of Combustion, 2011. **2011**(Article ID 528126): p. 20.
16. Horiba. *MEXA-1600/DEGR Specification*. 2012 08.11.2012]; Available from: http://www.horiba.com/automotive-test-systems/products/emission-measurement-systems/analytical-systems/standard-emissions/details/mexa-1600-degr-847/.
17. Horiba. *MEXA-1000 SPCS Specification*. 2012 08.11.2012]; Available from: http://www.horiba.com/automotive-test-systems/products/emission-measurement-systems/analytical-systems/particulates/details/mexa-1000-spcs-52/.
18. Dieselnet.com. *European Stationary Cycle (ESC)*. 2014 [cited 2014 07.08.2014]; Available from: https://www.dieselnet.com/standards/cycles/esc.php.
19. Kitano, K., I. Sakata, and R. Clark, *Effects of GTL fuel properties on DI diesel combustion.* SAE Technical Paper, 2005. **2005-01-3763**.
20. Wang, X., Z. Huang, O.A. Kuti, W. Zhang, and K. Nishida, *Experimental and analytical study on biodiesel and diesel spray characteristics under ultra-high injection pressure.* International Journal of Heat and Fluid Flow, 2010. **31**(4): p. 659-666.
21. Hartikka, T., M. Kuronen, and U. Kiiski, *Technical performance of HVO (Hydrotreated Vegetable Oil) in diesel engines.* SAE Technical Paper, 2012. **2012-01-1585**.
22. Schaberg, P., J. Botha, M. Schnell, H.-O. Hermann, N. Pelz, and R. Maly, *Emissions Performance of GTL Diesel Fuel and Blends with Optimized Engine Calibrations.* SAE Technical Paper, 2005. **2005-01-2187**.
23. Alleman, T.L. and R.L. McCormick, *Fischer-Tropsch diesel fuels-properties and exhaust emissions: A literature review.* SAE Technical Paper, 2003. **2003-01-0763**.
24. Azetsu, A., Y. Sato, and Y. Wakisaka, *Effects of aromatic components in fuel on flame temperature and soot formation in intermittent spray combustion.* SAE Technical Paper, 2003. **2003-01-1913**.
25. Su, T.F., C.T. Chang, R.D. Reitz, P.V. Farrell, A.D. Pierpont, and T.C. Tow, *Effects of injection pressure and nozzle geometry on spray SMD and DI emissions.* SAE Technical Paper, 1995. **952360**.

Table 1: Main fuel properties of HVO B100 and mineral diesel.

Fuel	Density at 15 °C [kg/m^3]	Viscosity at 40 °C [mm^2/s]	Cetane number (CN)	Calorific value [kJ/kg]	Aromatics content [%]	H/C molar ratio
B0 mineral diesel	840.4	2.82	51	42,853	27.5	1.88 : 1
HVO B100	780.1	3.02	>75	43,902	0	2.13 : 1

List of Figures

Figure 01
Click here to download high resolution image

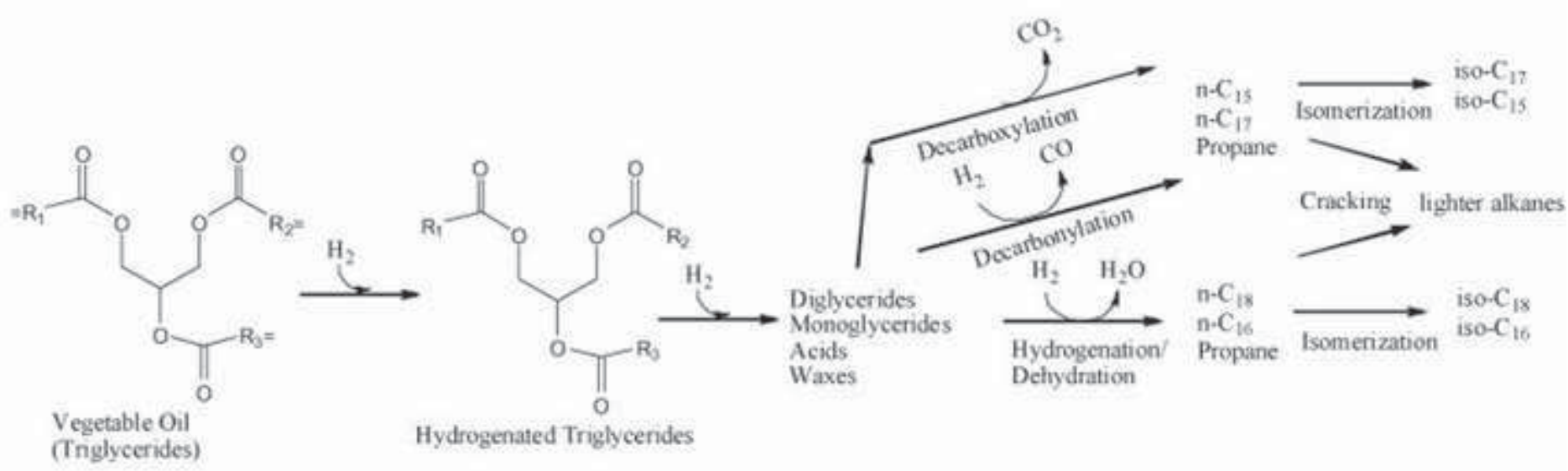

Figure 02

Click here to download high resolution image

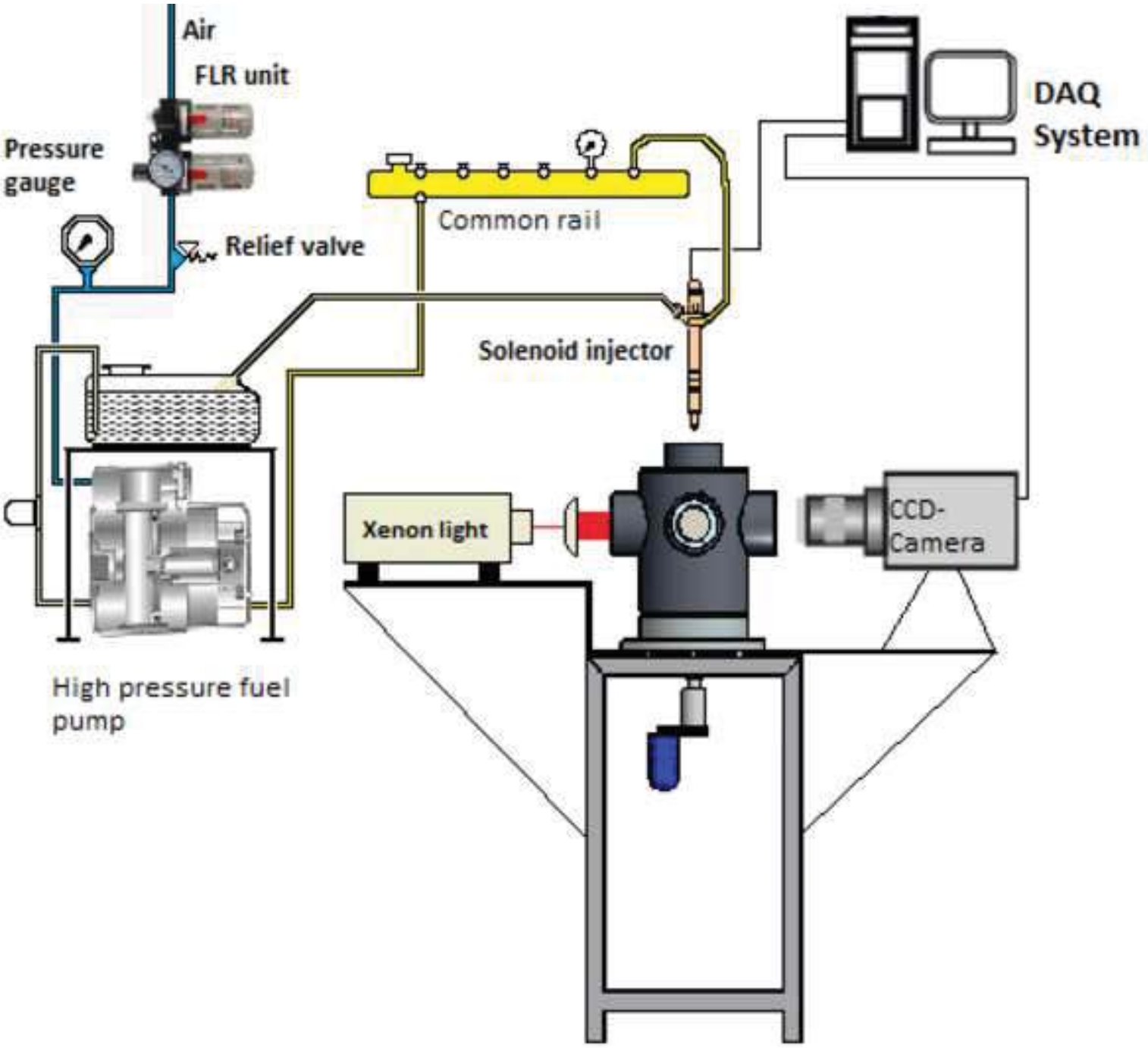

Figure 03
Click here to download high resolution image

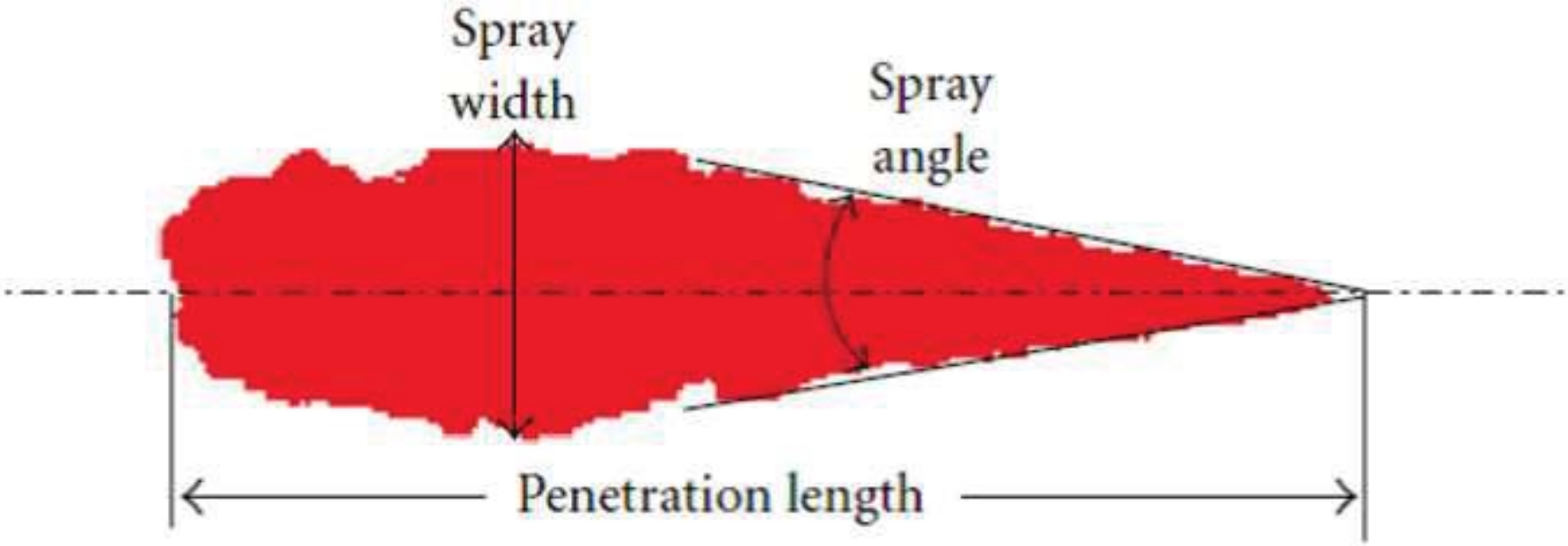

Figure 04
Click here to download high resolution image

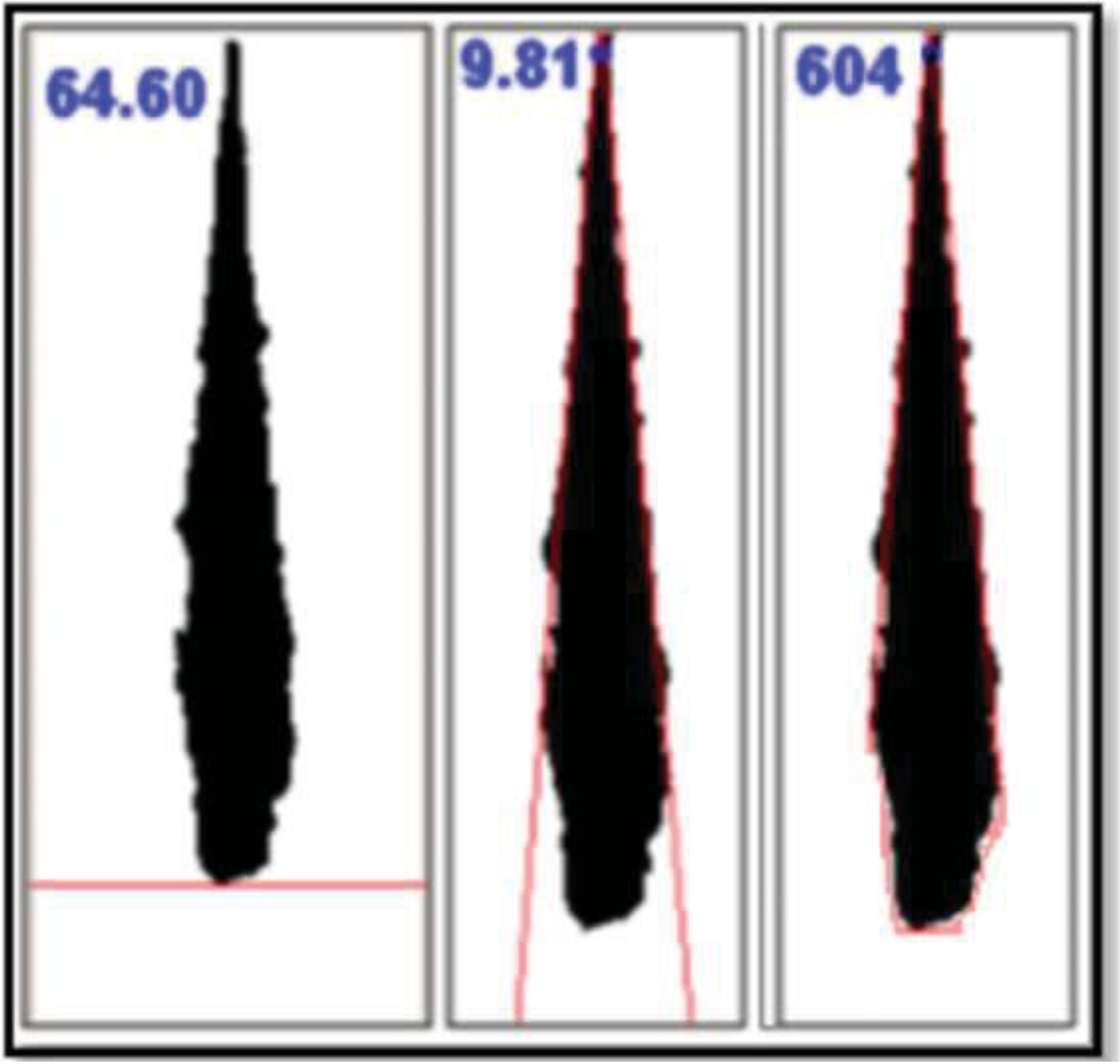

Figure 05
Click here to download high resolution image

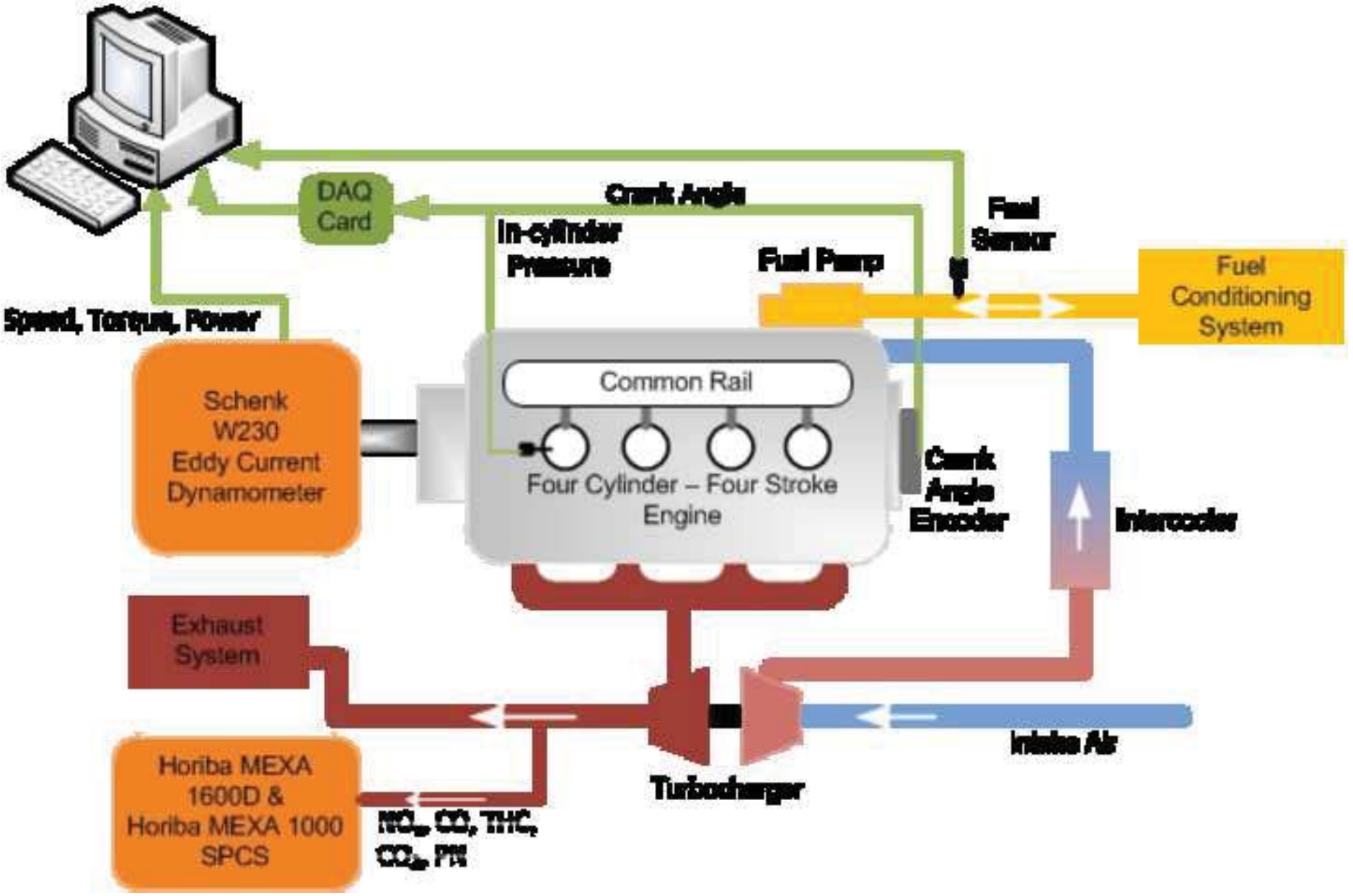

Figure 06

Click here to download high resolution image

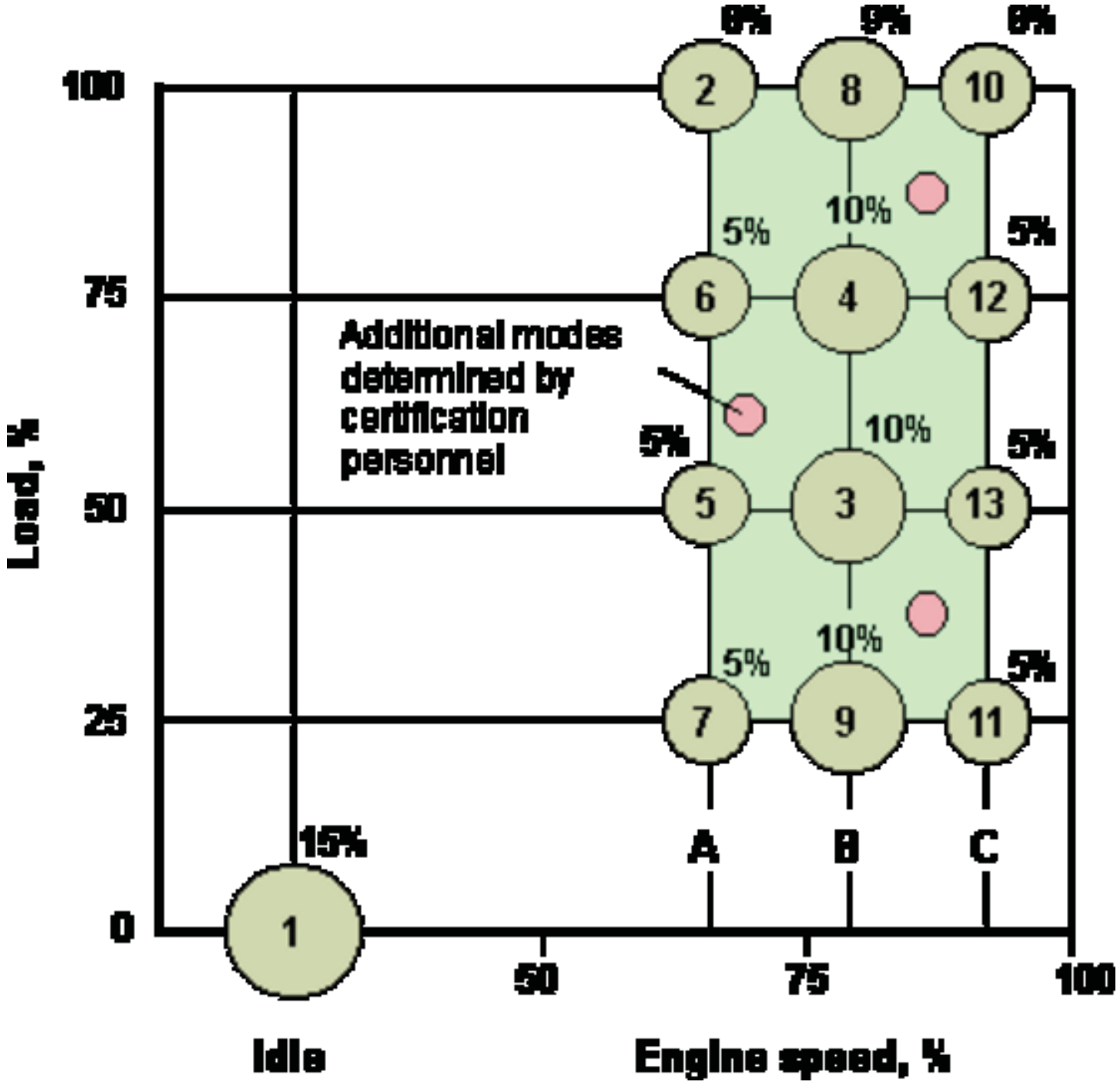

Figure 07

Click here to download high resolution image

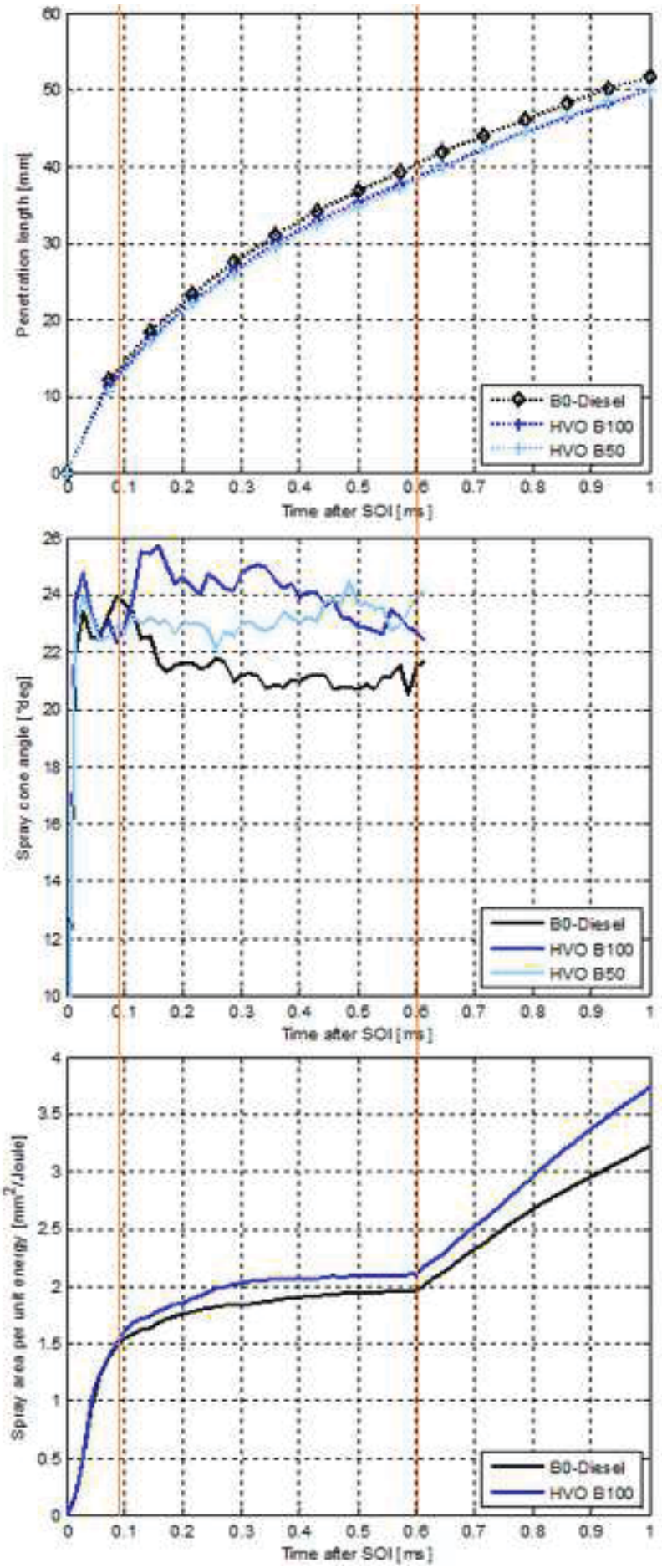

Figure 08
Click here to download high resolution image

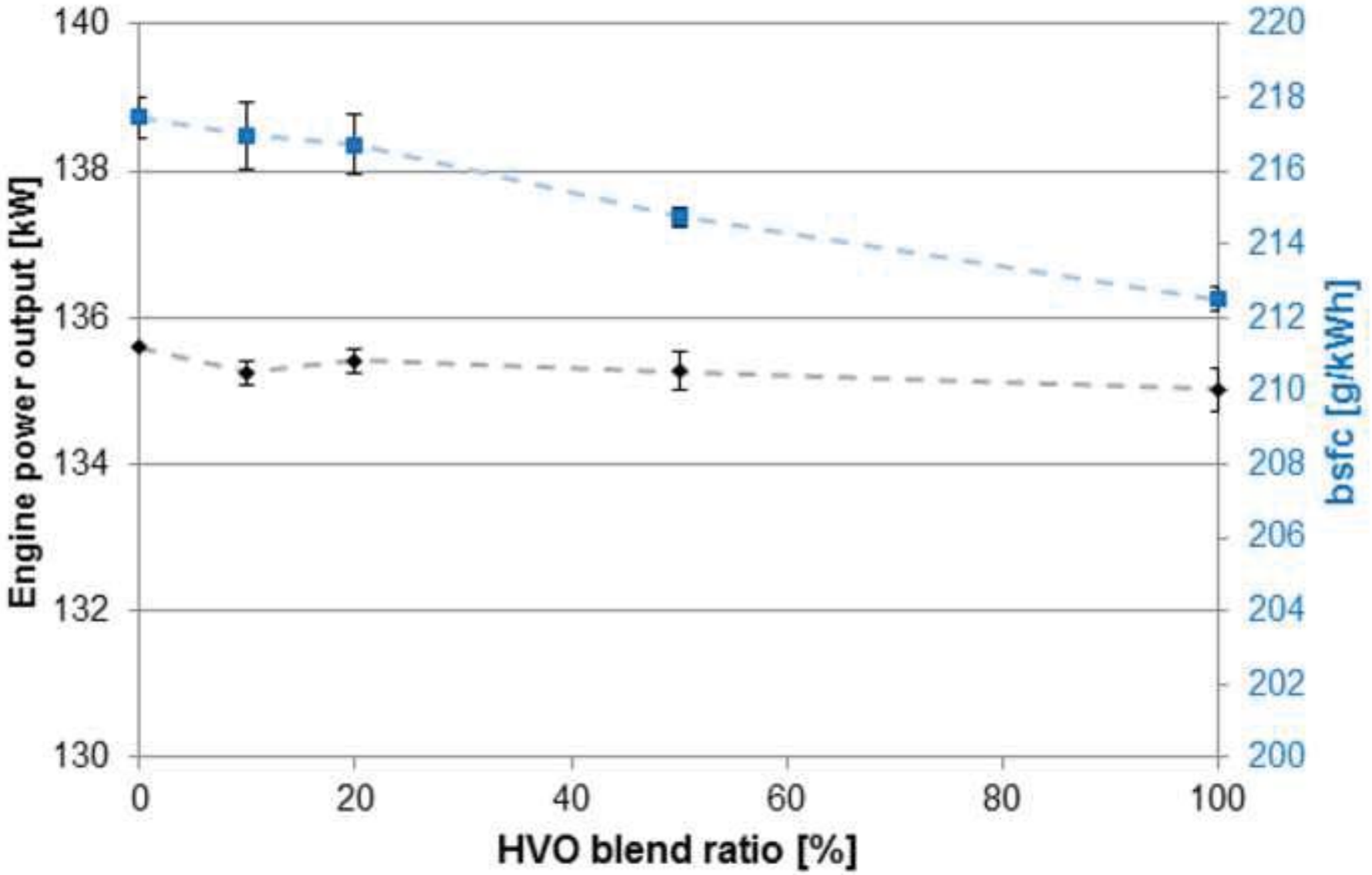

Figure 09
Click here to download high resolution image

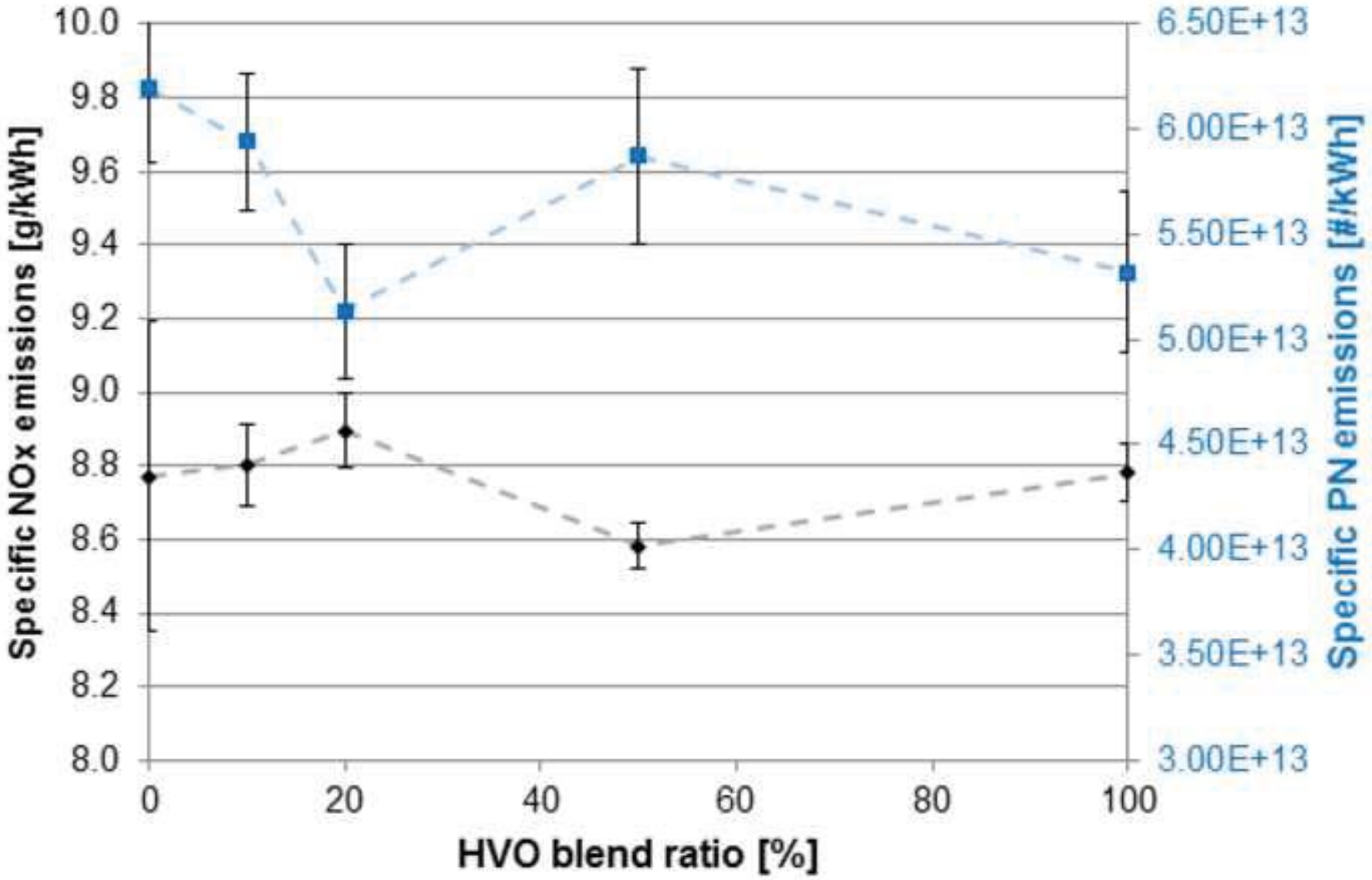

Figure 10
Click here to download high resolution image

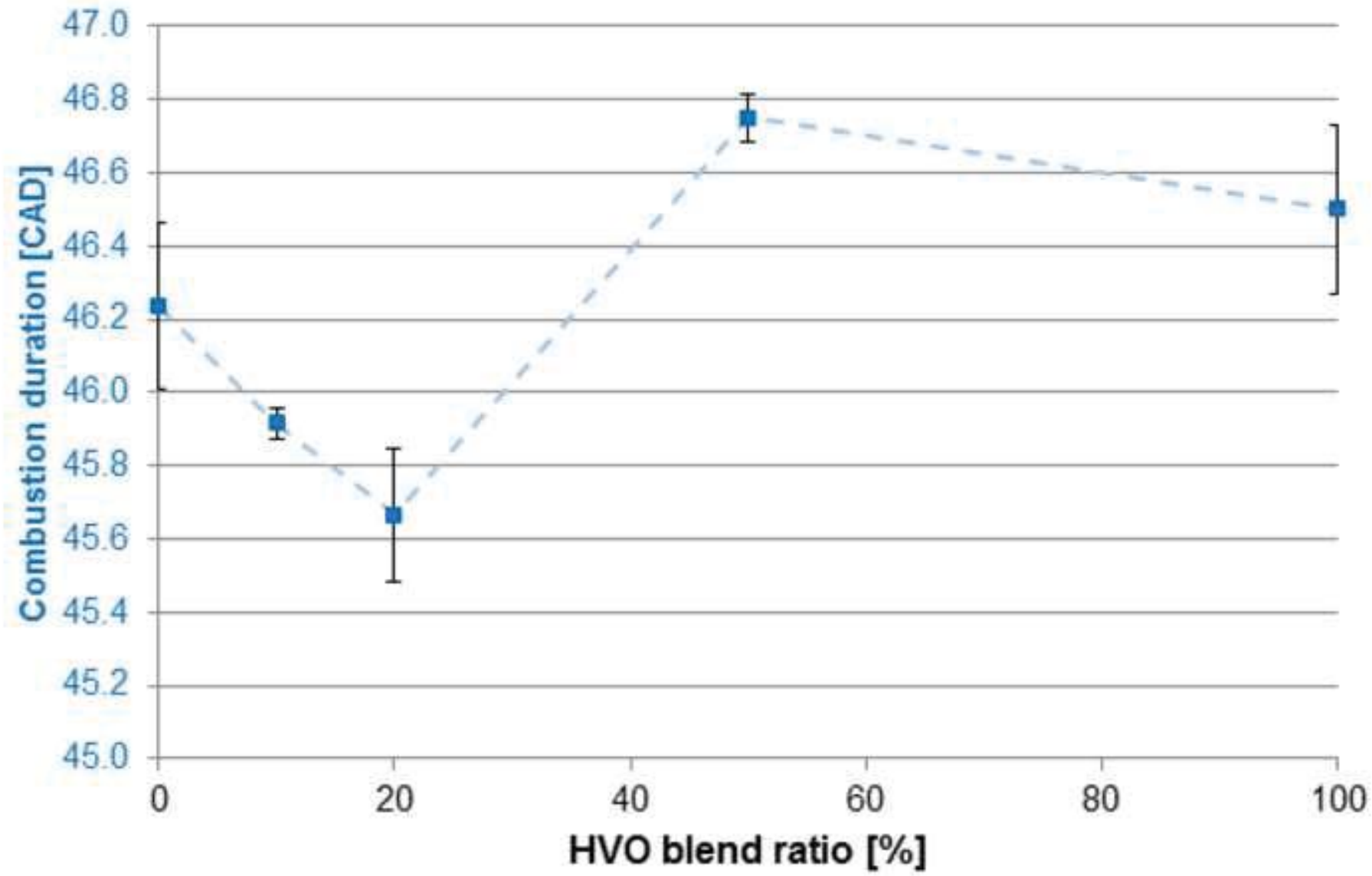

Figure 11
Click here to download high resolution image

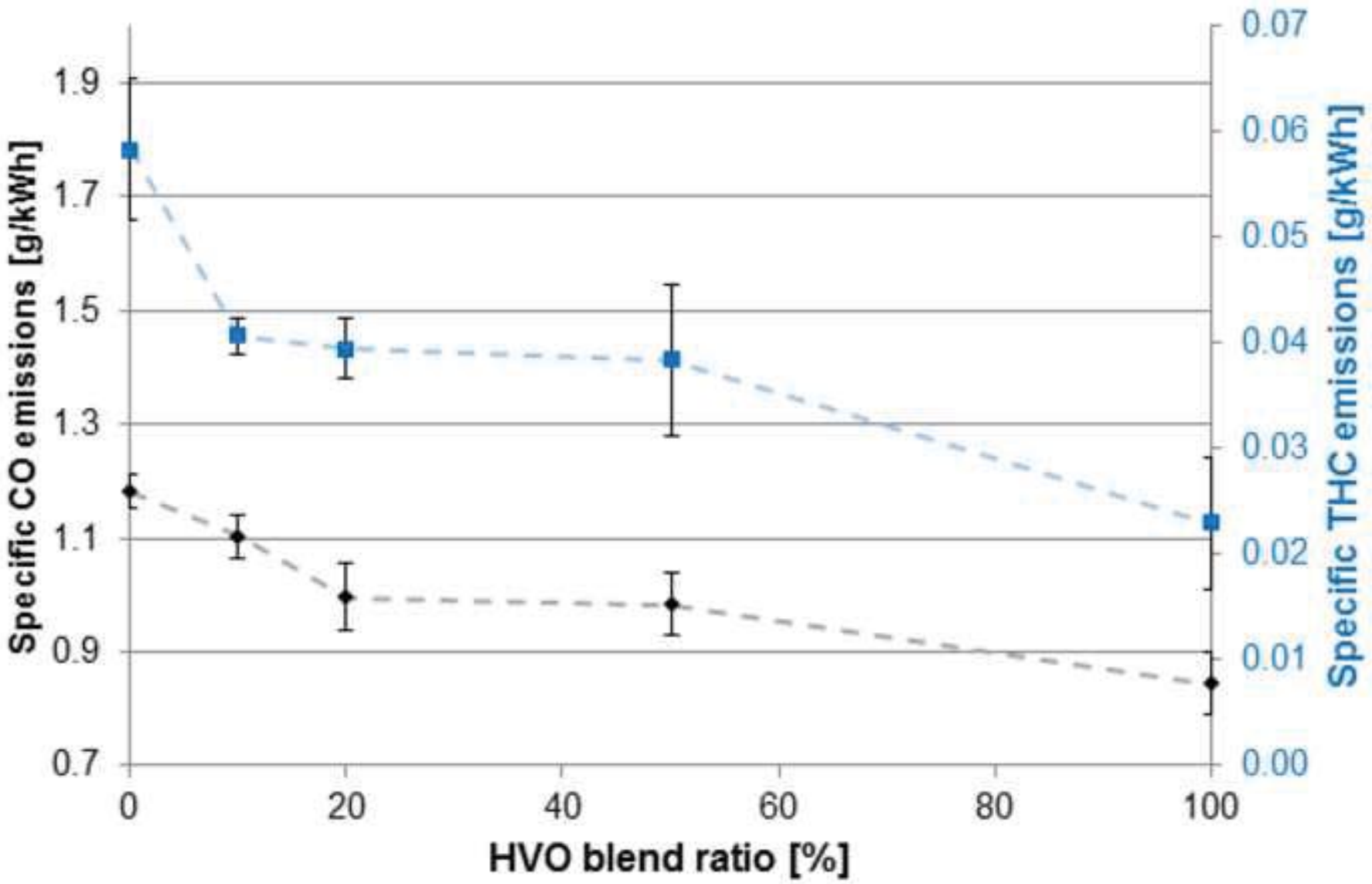

Figure 12
Click here to download high resolution image

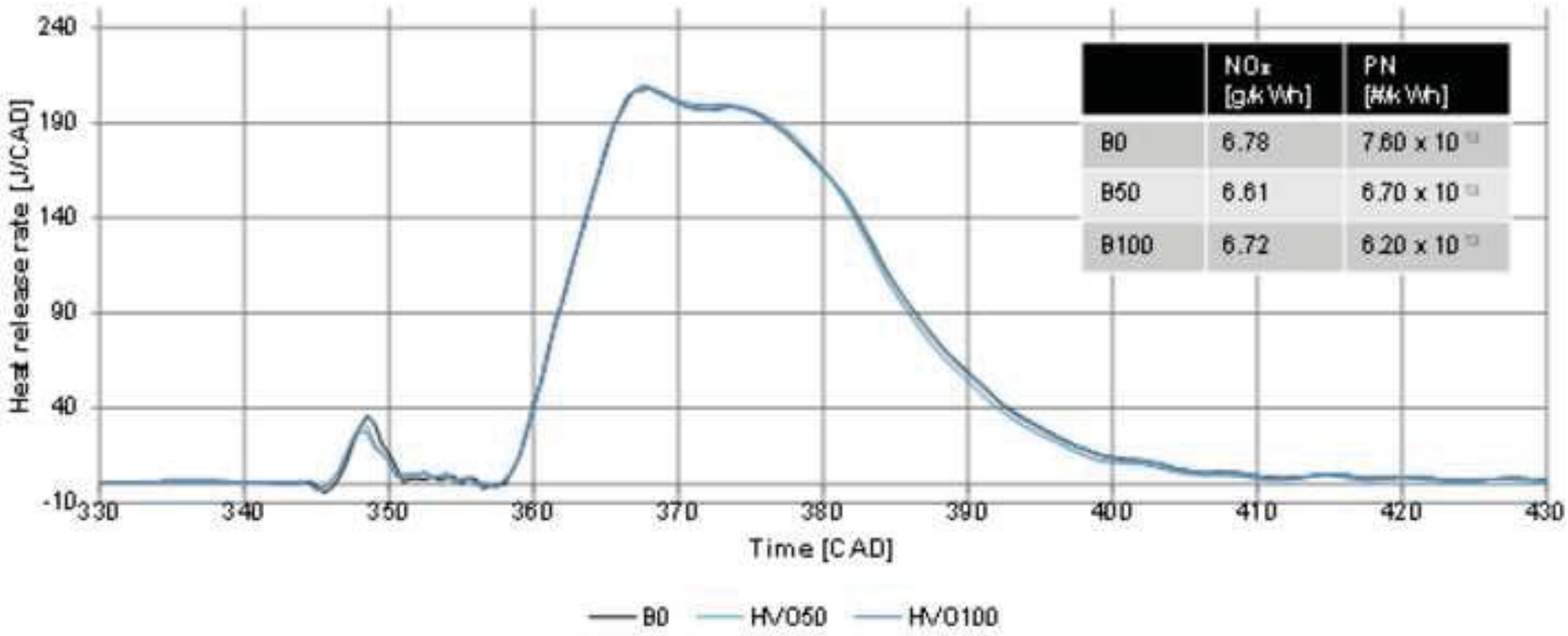

Figure 13
Click here to download high resolution image

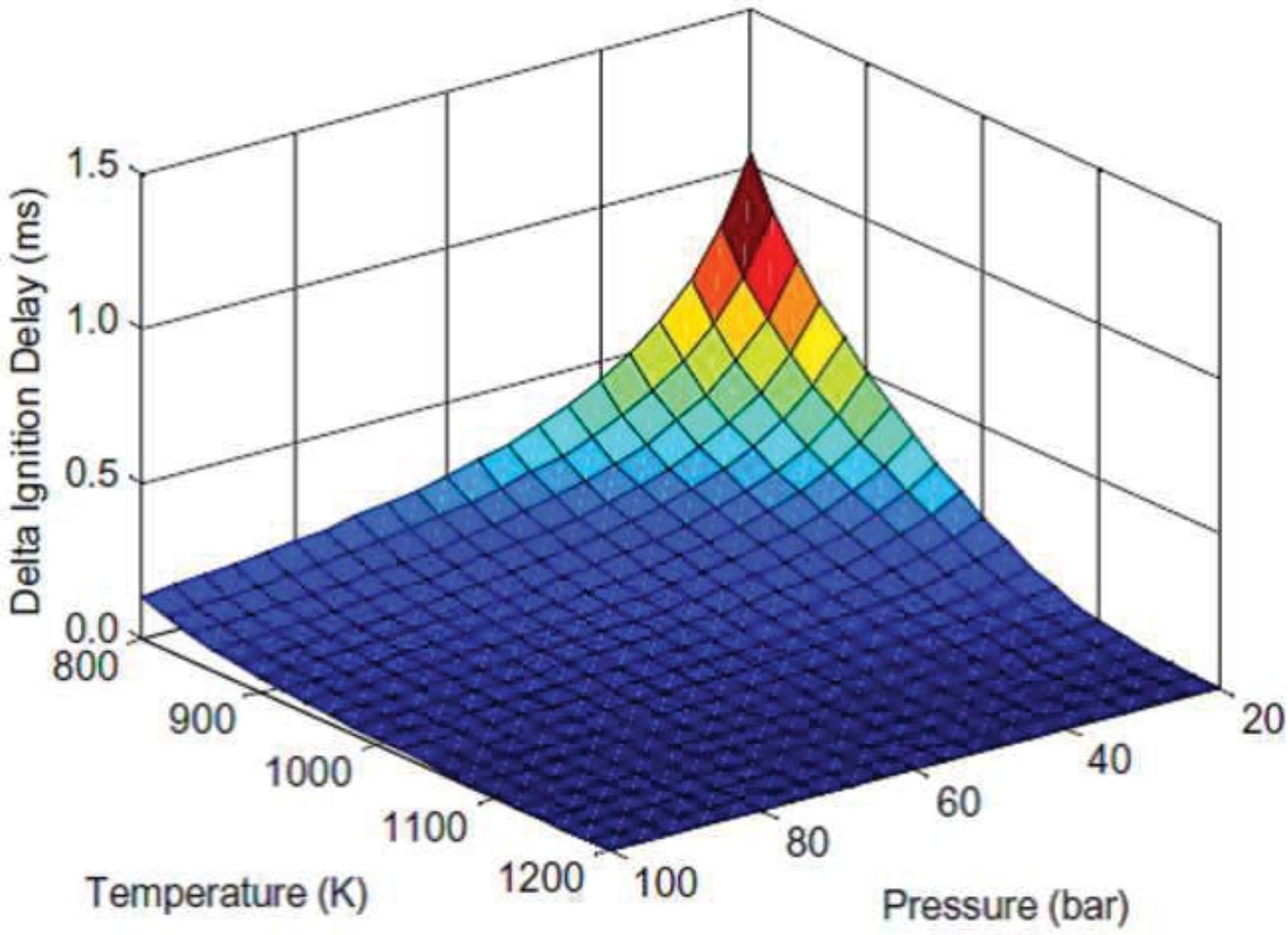

Figure 14
Click here to download high resolution image

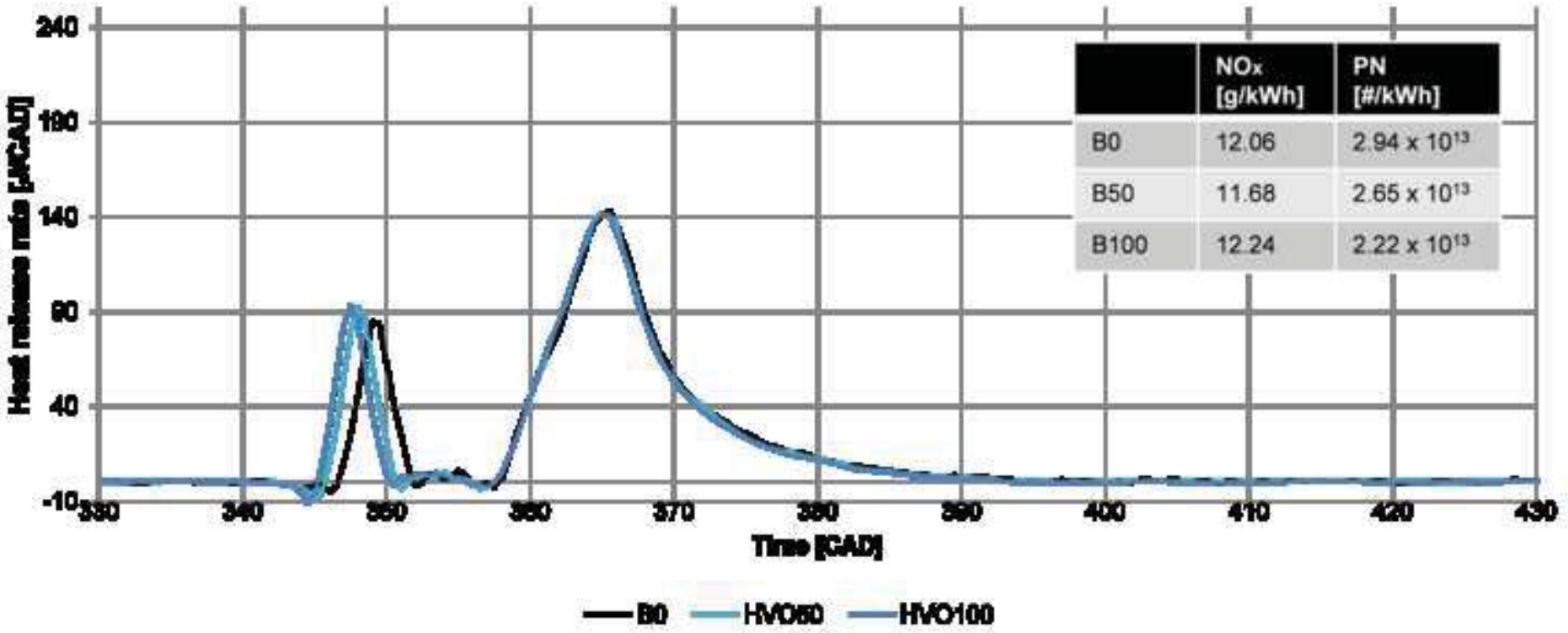

	NOx [g/kWh]	PN [#/kWh]
B0	12.06	2.94×10^{13}
B50	11.68	2.65×10^{13}
B100	12.24	2.22×10^{13}

Figure 15
Click here to download high resolution image

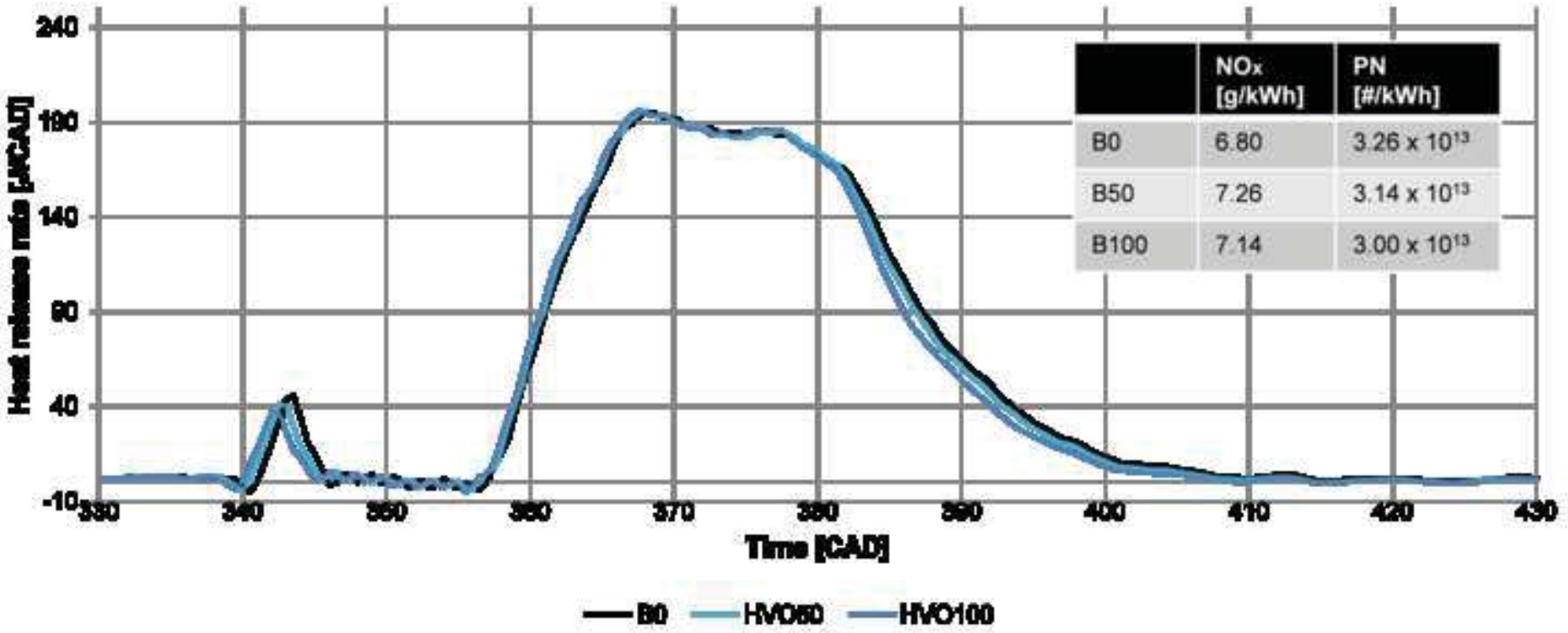

	NOx [g/kWh]	PN [#/kWh]
B0	6.80	3.26×10^{13}
B50	7.26	3.14×10^{13}
B100	7.14	3.00×10^{13}

Figure 16
Click here to download high resolution image

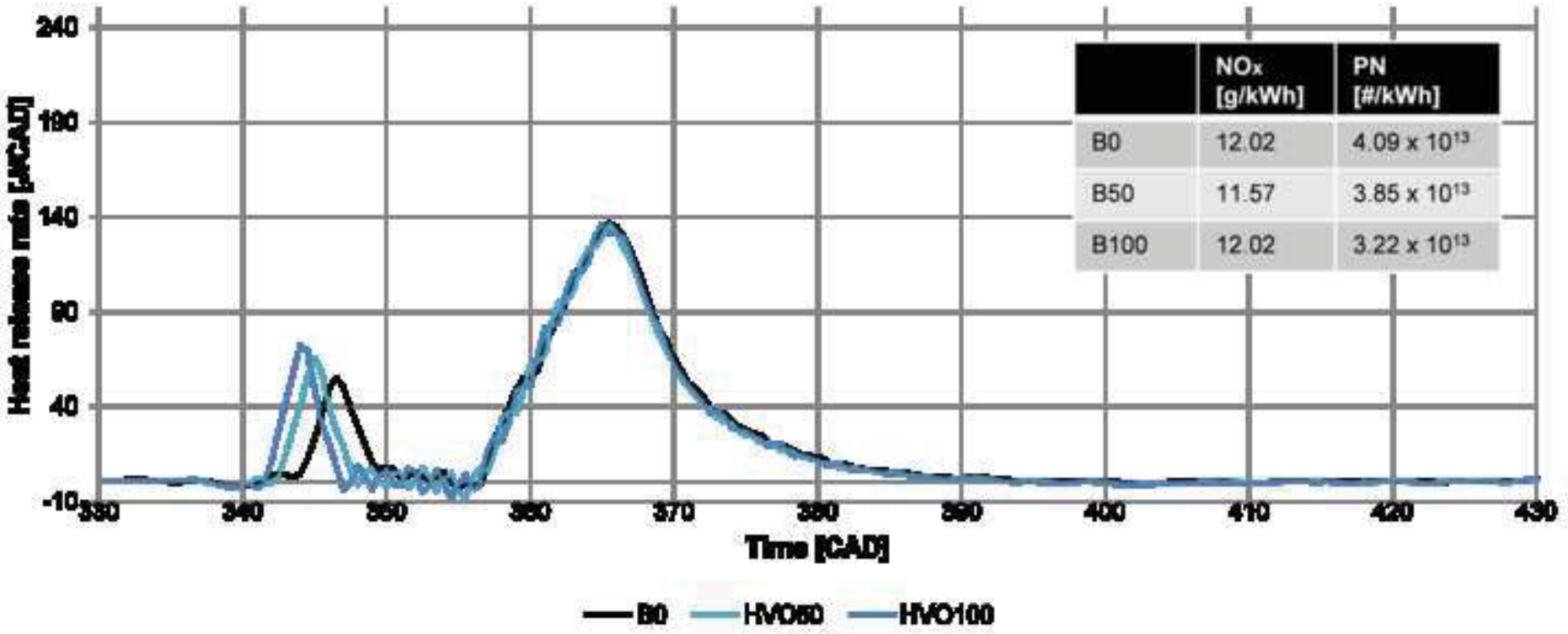

	NOx [g/kWh]	PN [#/kWh]
B0	12.02	4.09×10^{13}
B50	11.57	3.85×10^{13}
B100	12.02	3.22×10^{13}

Figure 17
Click here to download high resolution image

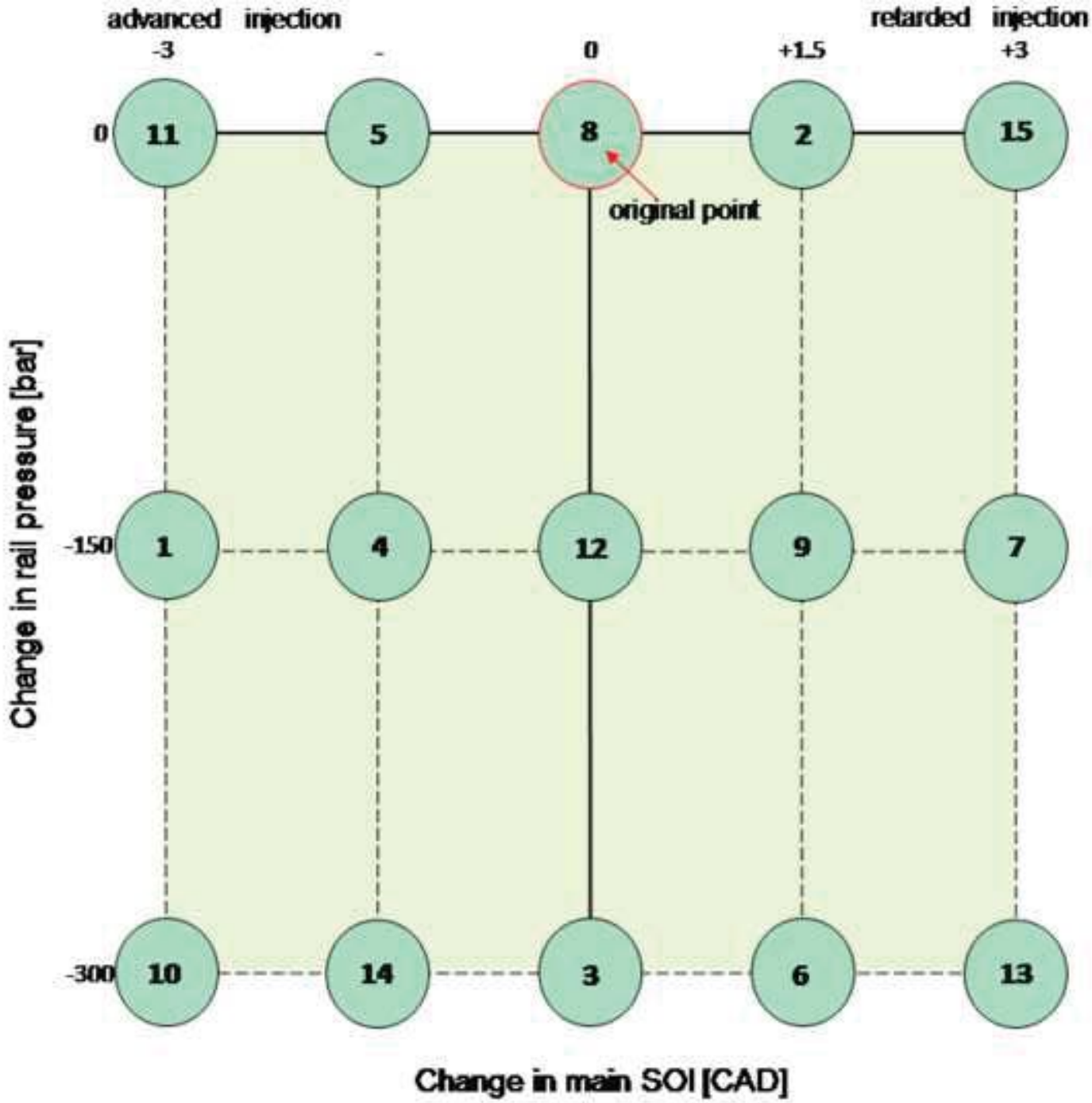

Figure 18
Click here to download high resolution image

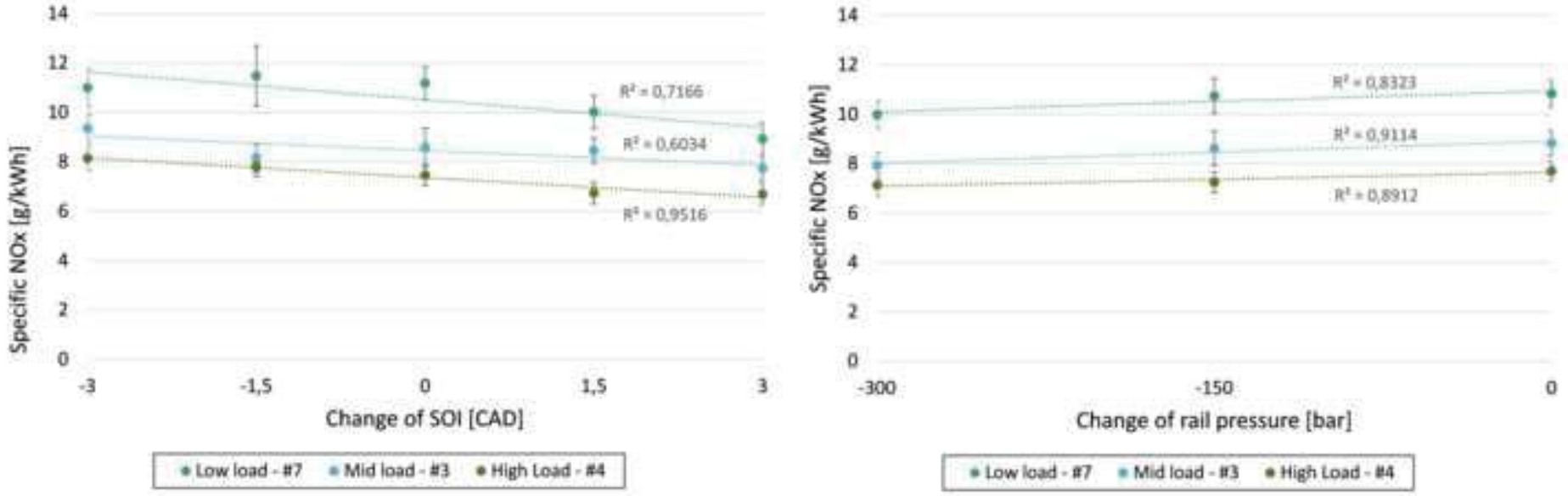

Figure 19
Click here to download high resolution image

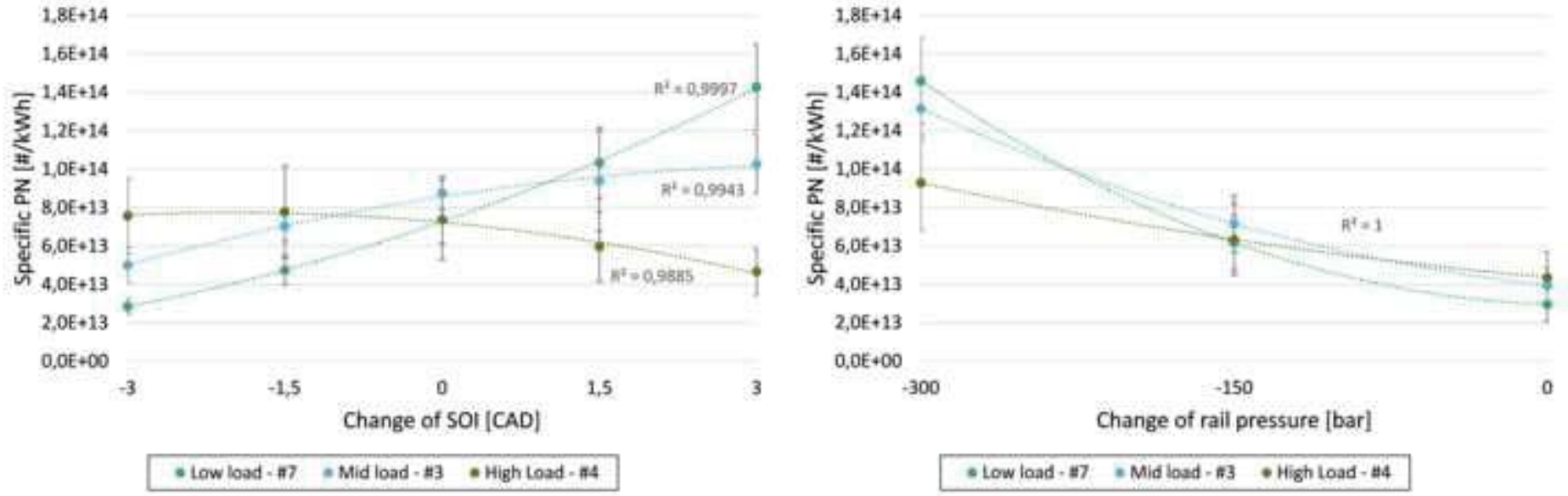

Figure 20
Click here to download high resolution image

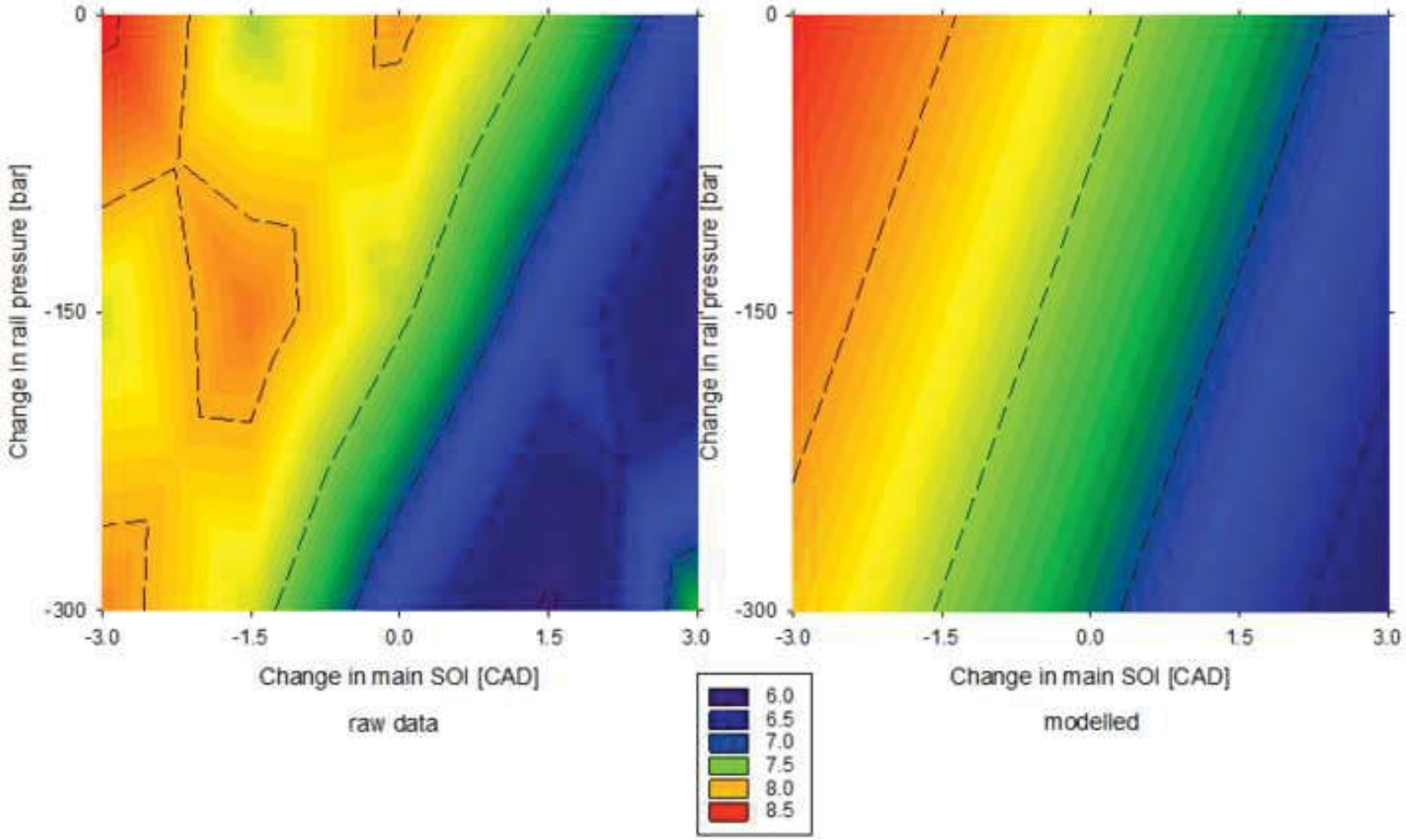

Figure 21
Click here to download high resolution image

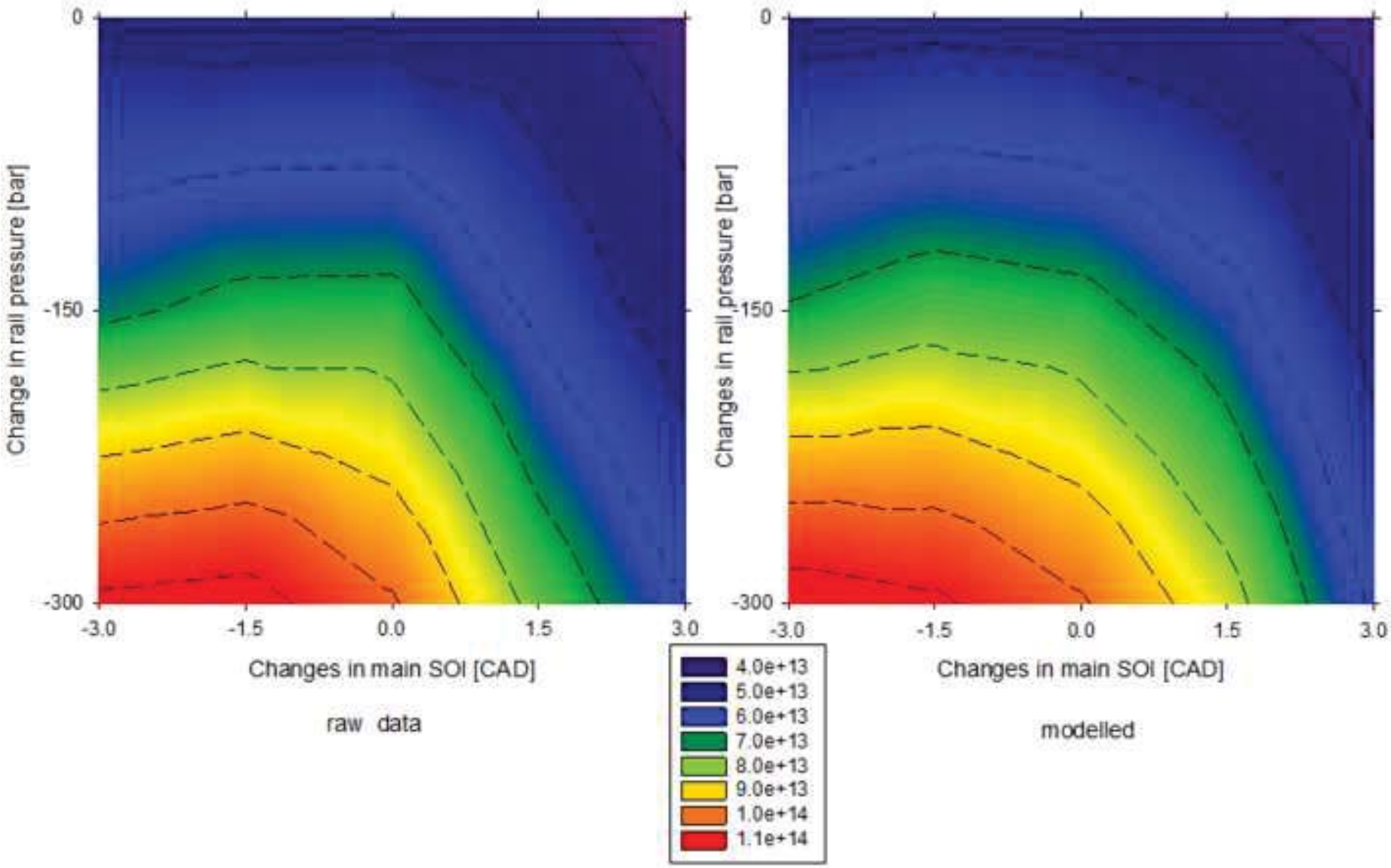

Figure 22
Click here to download high resolution image